Supporting Information

Phase Transition-Induced Band Edge Engineering of $BiVO_4$ to Split Pure Water under Visible Light

Won Jun Jo,[a] Hyun Joon Kang,[b] Ki-Jeong Kong,[c] Yun Seog Lee,[d] Hunmin Park,[b] Younghye Lee,[b] Tonio Buonassisi,[d] Karen K. Gleason,[a] and Jae Sung Lee[e,*]

[a]Department of Chemical Engineering, Massachusetts Institute of Technology, Cambridge, MA 02139, USA

[b]Department of Chemical Engineering, Pohang University of Science and Technology (POSTECH), Pohang, 790-784, Korea

[c]Korea Institute of Chemical Technology, Daejeon, 305-343, Korea

[d]Department of Mechanical Engineering, Massachusetts Institute of Technology, Cambridge, MA 02139, USA

[e]School of Energy and Chemical Engineering, Ulsan National Institute of Science and Technology (UNIST), Ulsan, 689-798, Korea

S1. Flat-band position and IPCE measurement with fabricated photoelectrodes

Photoelectrodes for flat-band potential and incident photon to charge carrier efficiency (IPCE) measurement were fabricated by typical electrophoretic deposition (EPD) method. The sample and iodine were added in acetone, and well dispersed by sonication and stirring. EPD was performed onto 1x1 cm^2 area of FTO glass (Pilkington, TEC 8, ~8Ω/square) at 55 V for 5 min with another FTO glass as a counter electrode. The photoelectrode was washed with absolute acetone after EPD and then sintered in a furnace at 400 °C for 30 min in the air. Copper wires were attached with silver paste and all exposed conducting parts except deposited

sample were covered with epoxy resin.

Mott-Schottky plot was obtained by using a potentiostat (IviumStat, Ivium Technologies) at applied frequency of 500 Hz under dark condition. The flatband potential (ϕ_{fb}) can be determined using the x-intercept of the following equation:

$$\frac{1}{C^2} = \left(\frac{2}{e\epsilon_0\epsilon_r N_d A^2}\right)\left(\phi - \phi_{fb} - \frac{kT}{e}\right)$$

where C is the differential capacitance of the space-charge region, ϵ_r is the relative dielectric constant of sample, ϵ_0 is the permittivity of the vacuum, N_d is the donor density, ϕ is the applied potential and k is the Boltzmann constant. The conduction band position is assumed to be same with the flatband potential for n-type semiconductor. The valence band position is induced by adding the band gap energy.

IPCE was evaluated utilizing a quantum efficiency measurement system (QEX7, PV Measurement) and potentiostat (Reference 600, Gamry) at 10 nm wavelength scanning rate with 5 second measurement. 3-electrode system was commonly used with Pt mesh, Ag/AgCl, and 0.5M Na_2SO_4 solution as a counter electrode, reference electrode, and electrolyte, respectively to estimate flat-band potential and IPCE.

S2. Quantum yield measurements

The quantum yield of the 10% (In, Mo)-doped sample was calculated by the chemical actinometry of potassium ferrioxalate ($K_3(Fe(C_2O_4)_3)\cdot 3H_2O$) (1, 2). For the preparation of $K_3(Fe(C_2O_4)_3)\cdot 3H_2O$, 1.5M $K_2C_2O_4$ and 1M $FeCl_3$ in water solution were mixed and recrystallized two times resulting in green precipitate. The solution of 6 mM $K_3(Fe(C_2O_4)_3)\cdot 3H_2O$ in 50 mM sulfuric acid solution was irradiated under the same condition as that for photocatalytic activity measurements for 2 minutes. The irradiated solution was mixed with $NaCH_3COO\cdot 3H_2O$ buffer solution and 0.1% 1,10-phenanthroline solution as a color indicator. Non-irradiated solution was also prepared for comparison. The absorbance at 510 nm of the final complex solution was measured by UV-Vis-NIR spectrophotometer (Cary 5000, Varian) with a cell of 1 cm length. Photon flux is given by:

$$q = \frac{\Delta A\, V_1\, V_3}{\Phi(\lambda)\varepsilon(\lambda)V_2\, l\, t}$$

where ΔA = absorbance difference between irradiated and non-irradiated solutions, V_1 = the irradiated volume, V_2 = the sampling volume for complexation with phenanthroline, V_3 = the final volume after the complexation, l = the optical pathlength of the irradiation cell, t = the irradiation time, $\Phi(\lambda)$ = the quantum yield of ferrous ion production (1.11 at 510nm), and $\varepsilon(\lambda)$ = absorption coefficient (11100 dm^3 mol^{-1} cm^{-1} at 510 nm). The final apparent quantum yield is given by:

$$\text{A. Q. Y. (\%)} = \frac{\text{Number of reacted electrons}}{\text{Number of incident photons}} \times 100$$

S3. Turnover number calculations

We have evaluated the turnover number for visible light-driven overall water splitting reactions shown in Figure 4 to justify the stability and durability of RuO_2 deposited on $GBVO_{0.10}$. Since it is difficult to define the active site exactly and to determine its number for photocatalytic reactions, the total number of species (RuO_2 or $GBVO_{0.10}$) is used for the calculation following the previous published reference (3). Thus, the obtained turnover numbers (TON) are low limits of the real value.

	$GBVO_{0.10}$ (Phase I) for 10 hrs	$RuO_2/GBVO_{0.10}$ (Phase II-IV) for 30 hrs	Heated $RuO_2/GBVO_{0.10}$ (Phase V) for 10 hrs
Tot. moles of H_2 produced (μmol)	23.05	374	142
Tot. $GBVO_{0.10}$ moles (mol)	9.40×10^{-4}	9.12×10^{-4}	9.12×10^{-4}
Tot. RuO_2 moles (mol)	-	6.76×10^{-5}	6.76×10^{-5}
TON w.r.t. $GBVO_{0.10}$	**0.0490**	**0.820**	**0.312**
TON w.r.t. RuO_2	-	**11.1**	**4.21**
TOF w.r.t. $GBVO_{0.10}$ (h^{-1})	0.00490	0.0273	0.0312
TOF w.r.t. RuO_2 (h^{-1})	-	0.370	0.421

Turnover number (TON) = [the number of produced hydrogen atoms] / [the total moles of RuO_2 or $GBVO_{0.10}$].

Turnover frequency (TOF) = TON/time.

Hence, on the most reasonable basis (the moles of co-catalyst RuO_2), the continuous operation in Phase II-IV correspond to TON of 11.1 and a turnover frequency of 0.37 h^{-1}.

S4. Lattice-strain evaluations

a. Volumetric strain method

The principle of volumetric strain method has already been described in detail elsewhere such as any relevant textbooks. The following description for volumetric strain is just a brief version of the contents from some lecture notes.

Strain is related to change in dimensions and shape of a material. When the deformation is along one axis, the most elementary definition of stain is

strain = change in length / original length

When a material is stretched, the change in length and the strain are positive. When it is stretched, the change in length and the strain are negative. This conforms with the signs of the stress which would accompany these strains, tensile stresses being positive and compressive stresses negative. Likewise, we define volumetric strain e as:

e = change in volume / original volume

The volumetric strain is simply related to the normal strains. Consider a rectangular solid, whose original volume is given by $V_0 = xyz$. When the solid is deformed, the resulting volume is given by

$$V = x(1 + \varepsilon_x)y(1 + \varepsilon_y)z(1 + \varepsilon_z) = xyz(1 + \varepsilon_x + \varepsilon_y + \varepsilon_z + \varepsilon_x \varepsilon_y + \varepsilon_x \varepsilon_z + \varepsilon_y \varepsilon_z + \varepsilon_x \varepsilon_y \varepsilon_z)$$

If $| \varepsilon_x | < 1$ & $| \varepsilon_y | < 1$ & $| \varepsilon_z | < 1$,

$$V \approx xyz(1 + \varepsilon_x + \varepsilon_y + \varepsilon_z) = V_0(1 + \varepsilon_x + \varepsilon_y + \varepsilon_z)$$

Now, the volumetric strain becomes

$$e = (V - V_0) / V_0 = \varepsilon_x + \varepsilon_y + \varepsilon_z$$

b. Williamson-Hall method

The crystallite size (D) can be calculated using the Scherrer's equation (4):

$D = k\lambda / (\beta_D \cos\theta)$

where k is the shape coefficient (0.9), λ is the wavelength of the incident radiation (1.541874 nm), β_D is the peak broadening due to small crystallite size, and θ is the Bragg angle. β_D can be expressed as (5)

$$\beta_D^2 = \beta_{measures}^2 - \beta_{instrumental}^2$$

where $\beta_{measures}$ is the measured peak broadening from XRD patterns, $\beta_{instrumental}$ is the instrumental peak broadening. The peak broadening (β_S) due to lattice strain ($\varepsilon = \Delta d/(2d)$) can be estimated as (5)

$$\beta_S = 4\varepsilon \tan\theta$$

By using the Williamson-Hall plotting method, the contribution of crystallite size and lattice strain can be separated (6).

$$\beta\cos\theta = k\lambda/D + 4\varepsilon \sin\theta$$

where β is the sum of the peak broadenings due to the lattice strain and crystallite size ($\beta = \beta_D + \beta_S$).

Supplementary Figures

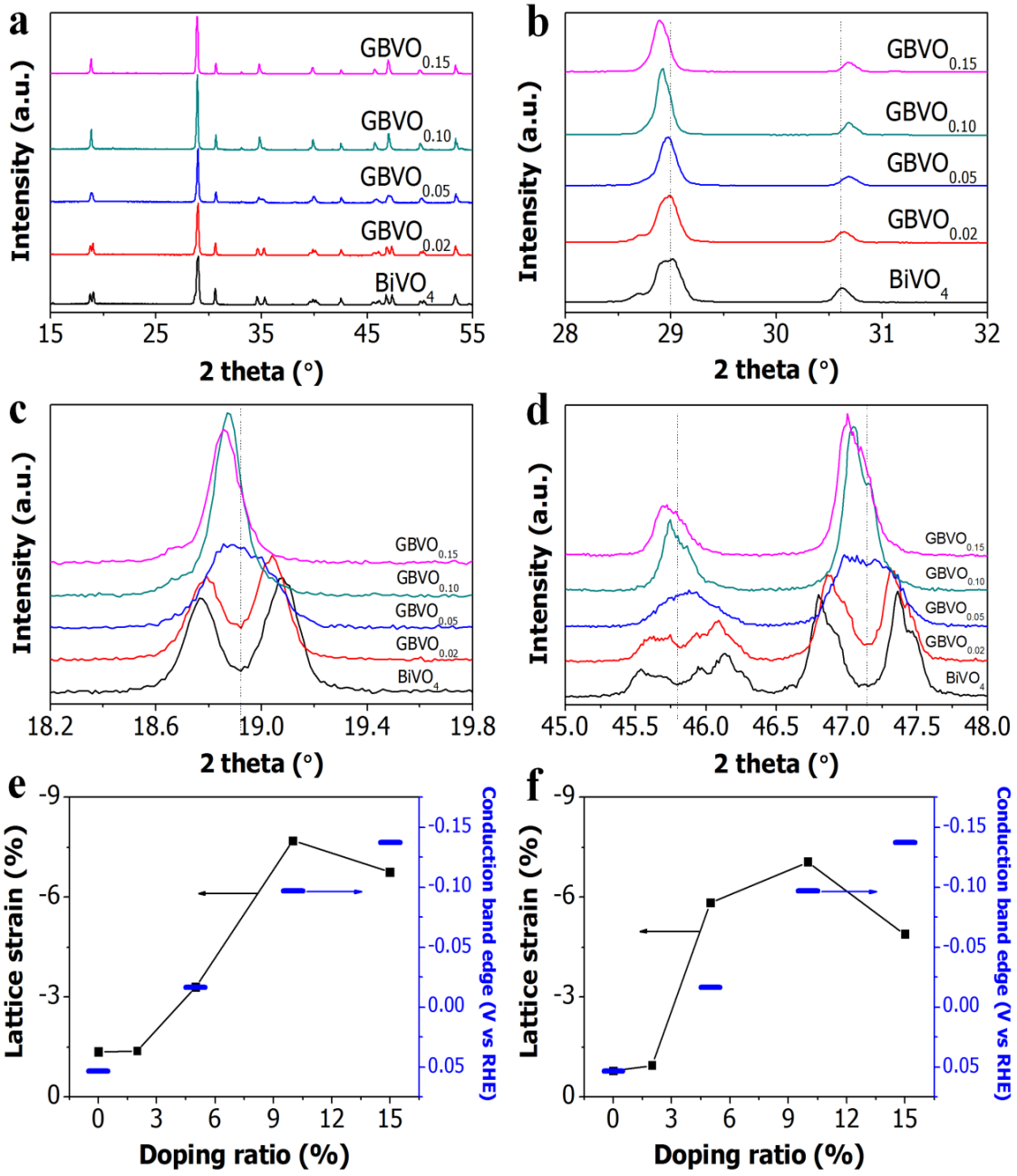

Figure S1. Shifts and evolution of XRD peaks, and relationship between lattice strain and conduction band edge: a) Full range XRD patterns, b) Main peaks' shift, and c) & d) Mergence of main peaks of pristine $BiVO_4$ and all $GBVO_x$ samples. e) Compressive (minus) lattice strain evaluated by volumetric strain method and conduction band edge position as a function of doping concentration. f) Compressive (minus) lattice strain evaluated by Williamson-Hall method and conduction band edge position as a function of doping concentration.

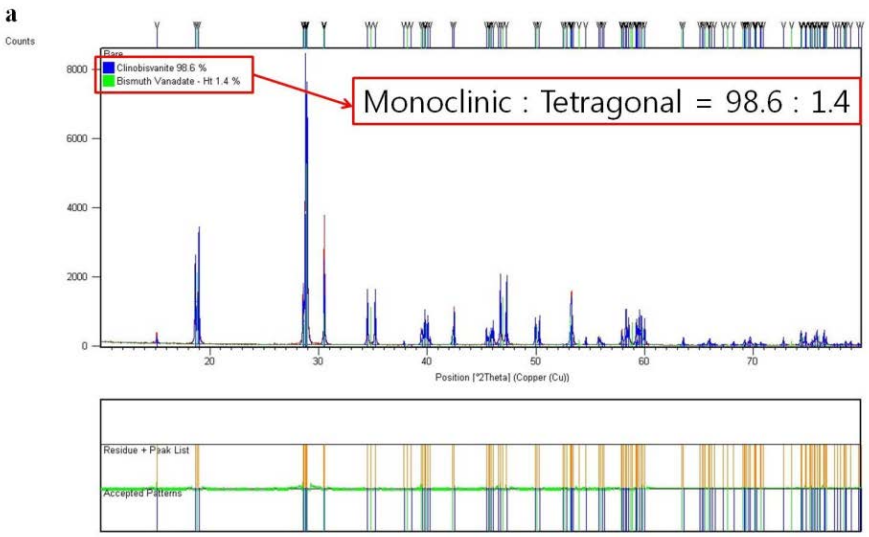
a
Counts
Clinobisvanite 98.6 %
Bismuth Vanadate - Ht 1.4 %
Monoclinic : Tetragonal = 98.6 : 1.4
Position [°2Theta] (Copper (Cu))
Residue + Peak List
Accepted Patterns

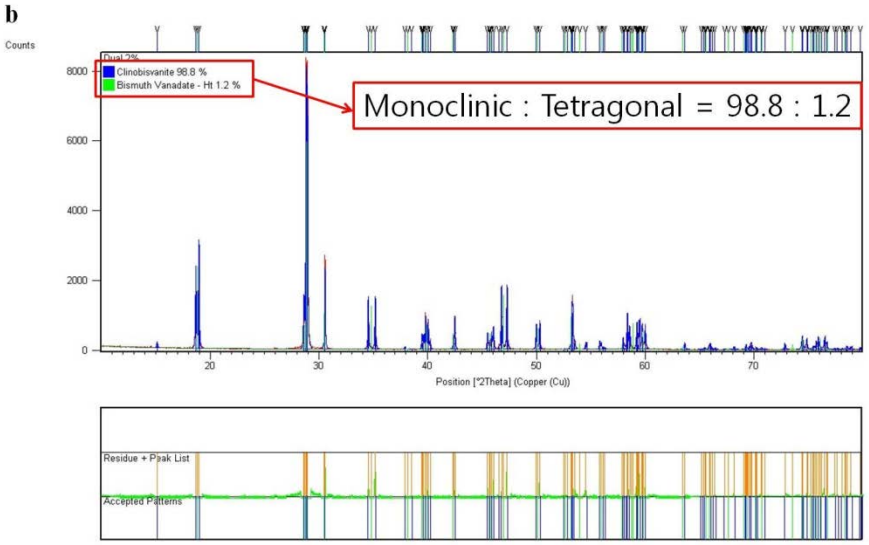
b
Counts
Clinobisvanite 98.8 %
Bismuth Vanadate - Ht 1.2 %
Monoclinic : Tetragonal = 98.8 : 1.2
Position [°2Theta] (Copper (Cu))
Residue + Peak List
Accepted Patterns

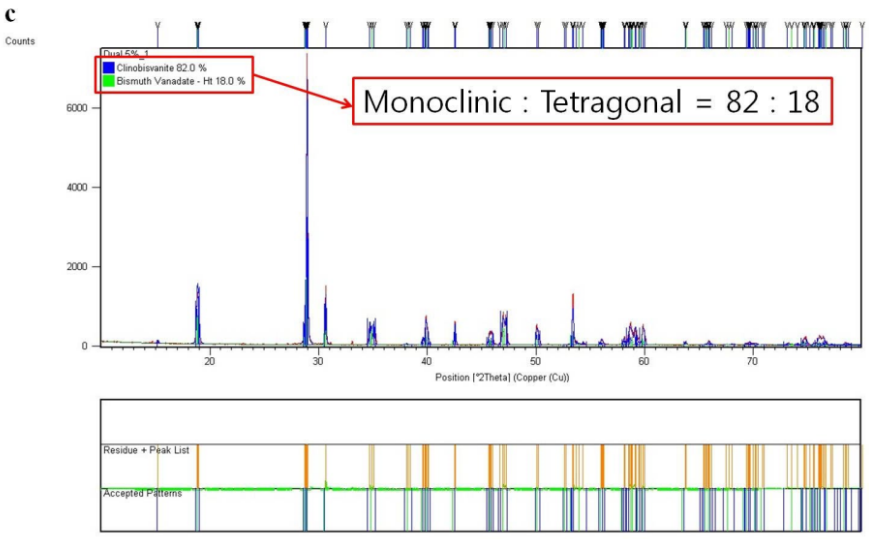
c
Counts
Clinobisvanite 82.0 %
Bismuth Vanadate - Ht 18.0 %
Monoclinic : Tetragonal = 82 : 18
Position [°2Theta] (Copper (Cu))
Residue + Peak List
Accepted Patterns

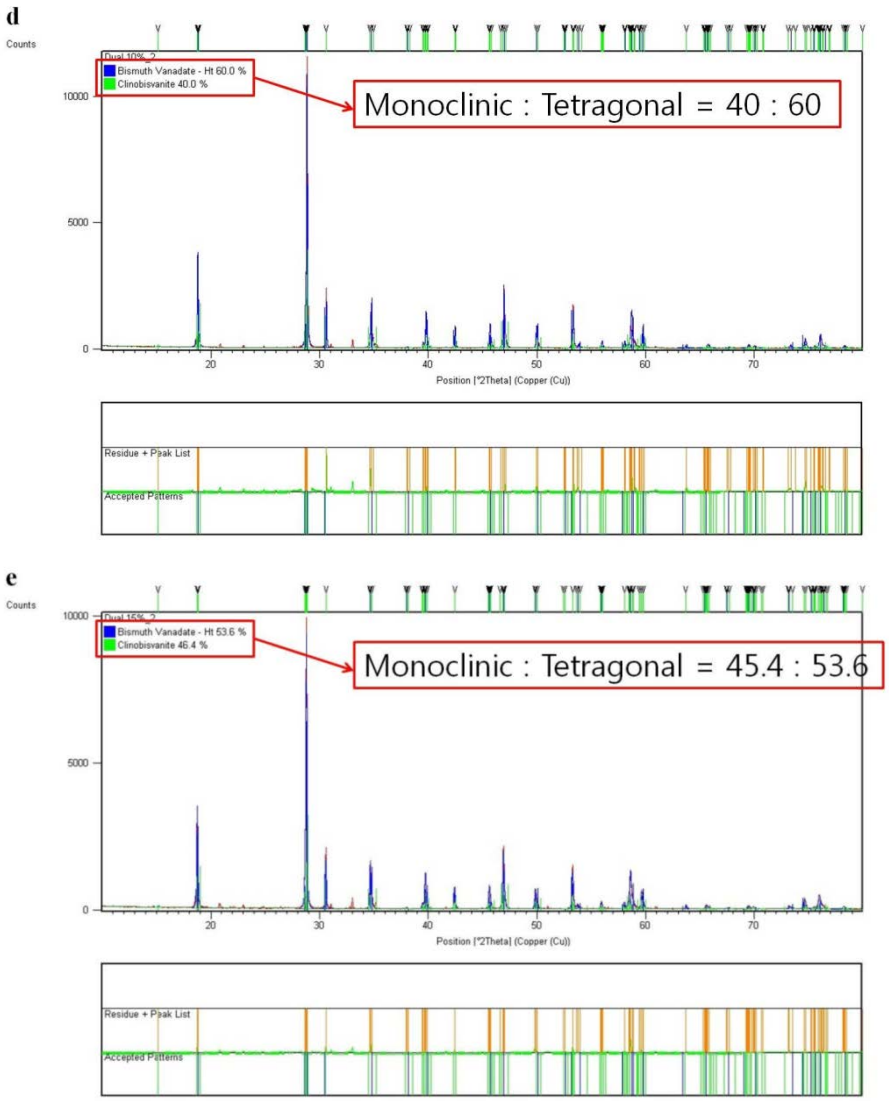

Figure S2. Monoclinic to tetragonal ratios in pristine $BiVO_4$ and all $GBVO_x$ samples. Blue colored peaks: Scheelite-monoclinic-$BiVO_4$ reference peaks. Green colored peaks: Tetragonal-$BiVO_4$ reference peaks. Orange colored peaks: Prepared-samples' peaks. a) Pristine $BiVO_4$, b) $GBVO_{0.02}$, c) $GBVO_{0.05}$, d) $GBVO_{0.10}$, e) $GBVO_{0.15}$.

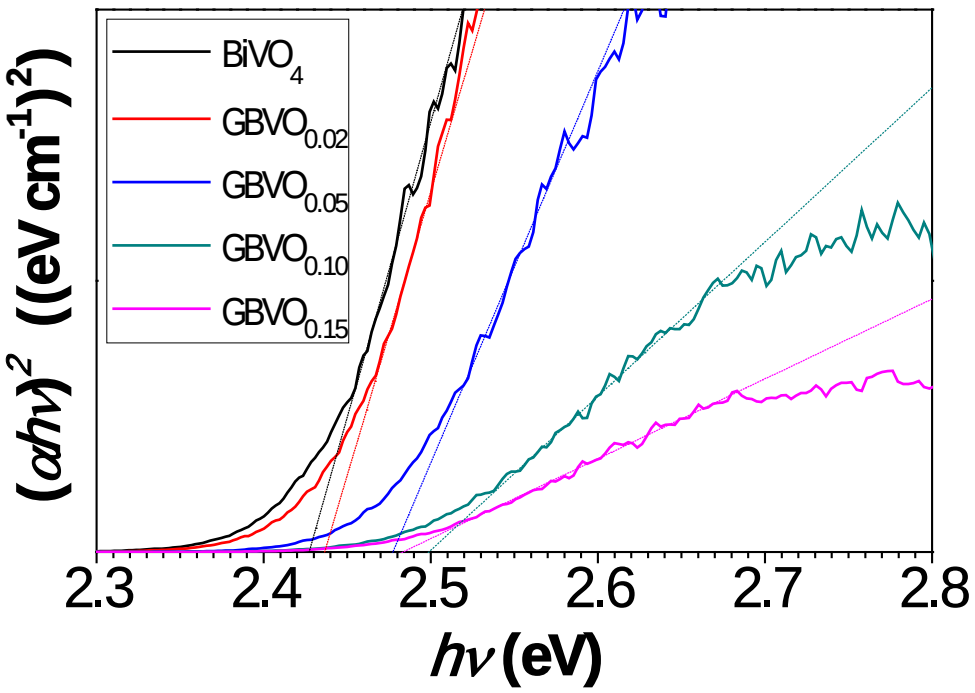

Figure S3. Tauc plot of pristine $BiVO_4$ and all $GBVO_x$ samples.

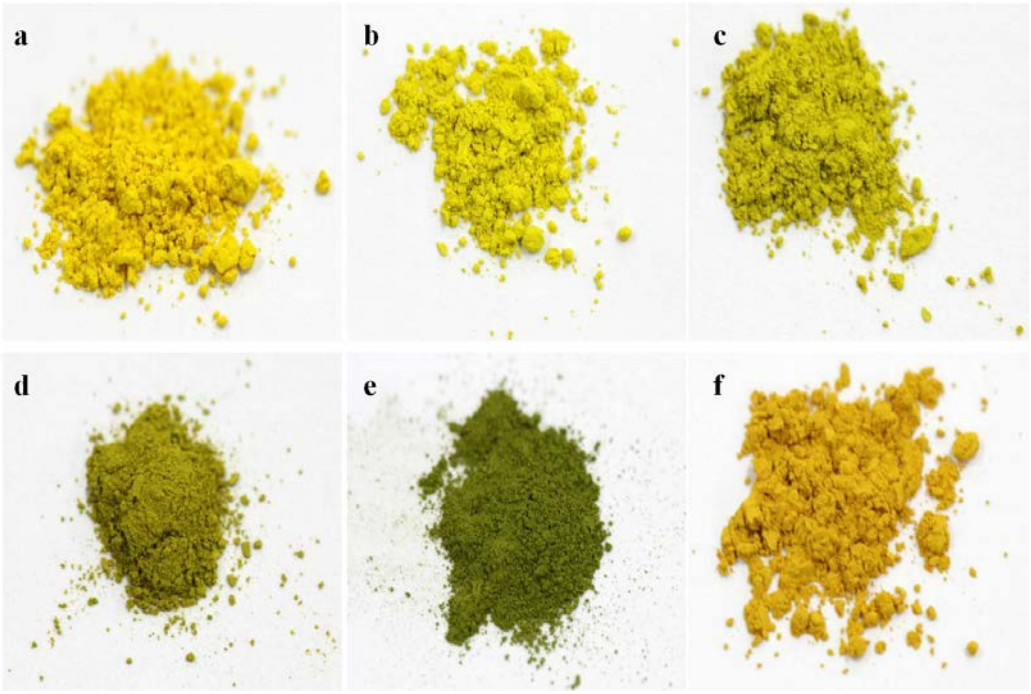

Figure S4. Powder sample images of pristine $BiVO_4$ and all $GBVO_x$ samples. a) Pristine $BiVO_4$, b) $GBVO_{0.02}$, c) $GBVO_{0.05}$, d) $GBVO_{0.10}$, e) $GBVO_{0.15}$, f) $BiV_{0.98}Mo_{0.02}O_4$.

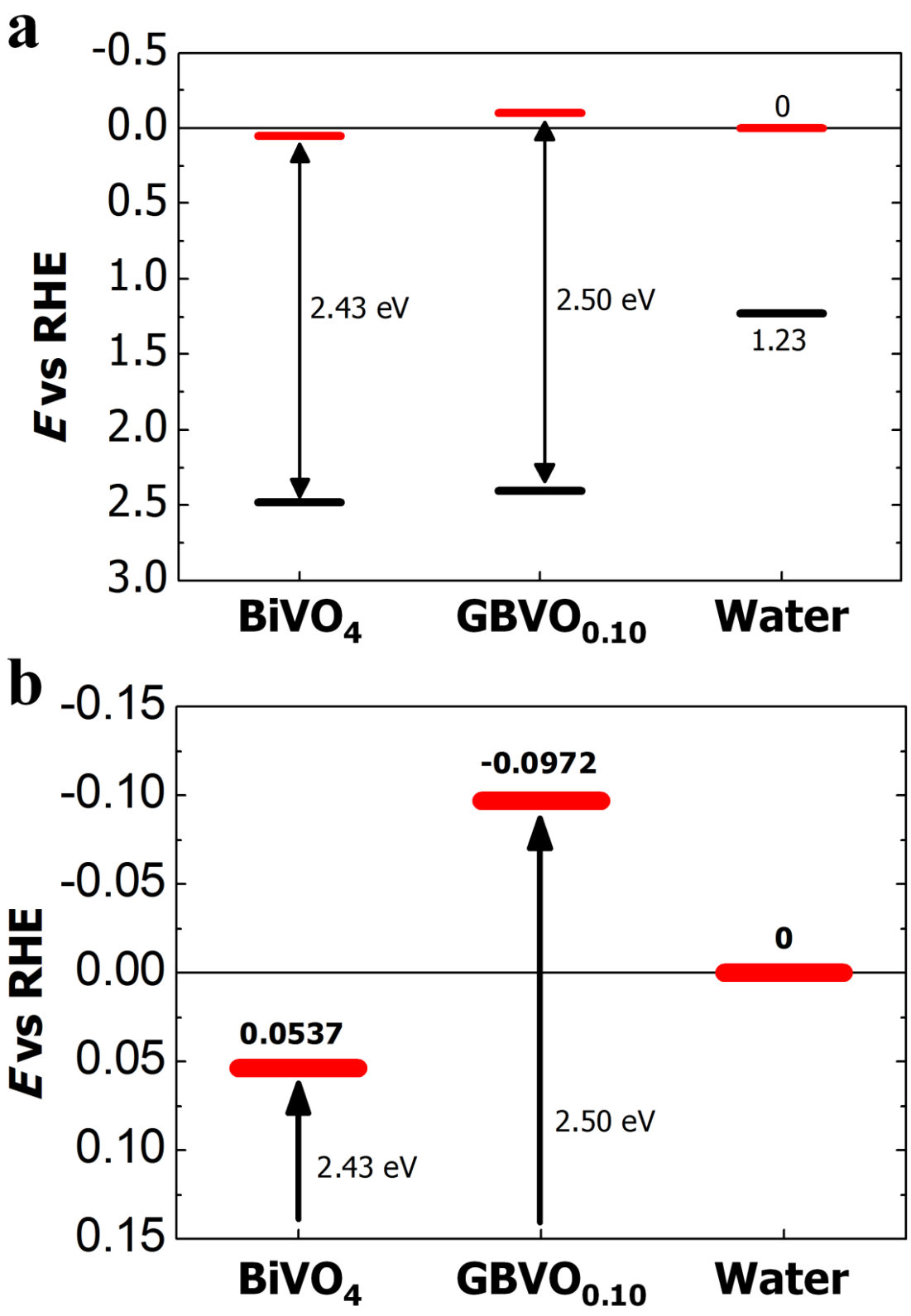

Figure S5. Band structures determined by Tauc and Mott-Schottky plots for Pristine $BiVO_4$ and $GBVO_{0.10}$. a) Overall band structure, b) Blow-up near conduction band edge.

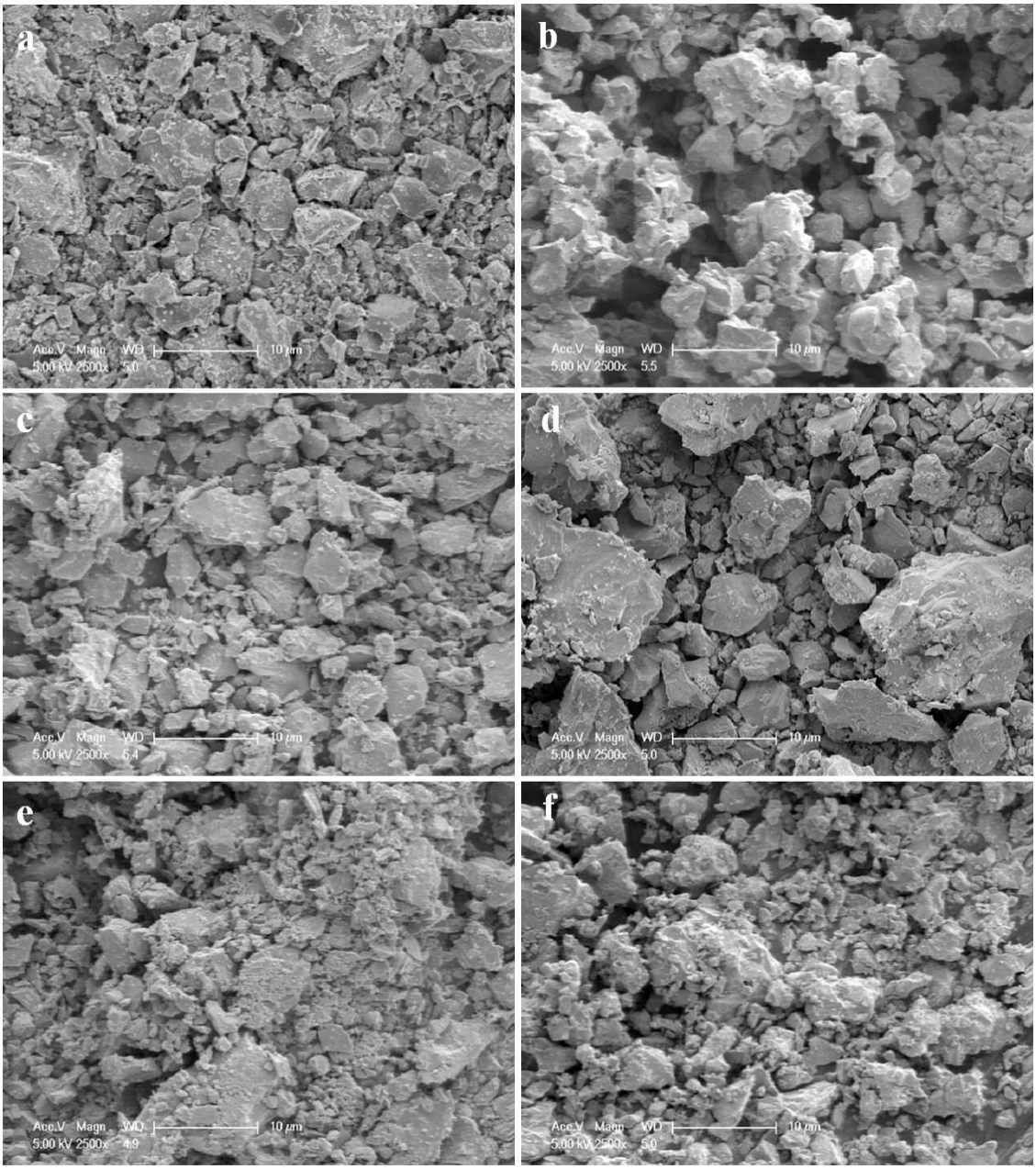

Figure S6. FESEM images of pristine $BiVO_4$ and all $GBVO_x$ samples. a) Pristine $BiVO_4$, b) $GBVO_{0.02}$, c) $GBVO_{0.05}$, d) $GBVO_{0.10}$, e) $GBVO_{0.15}$, f) $BiV_{0.98}Mo_{0.02}O_4$.

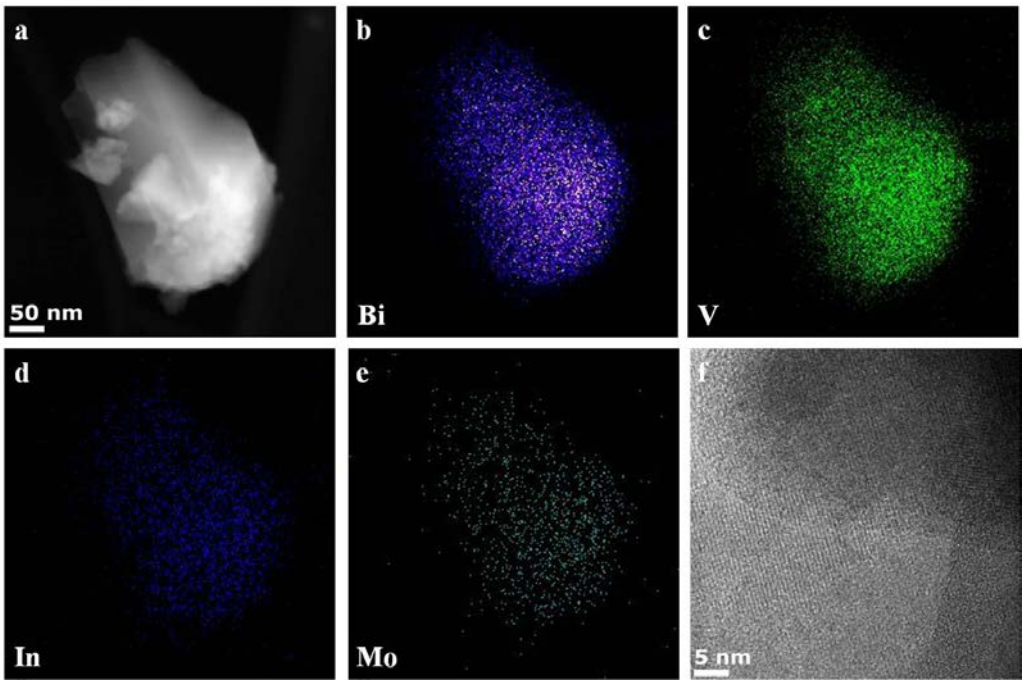

Figure S7. HR-TEM EDS analysis of $GBVO_{0.02}$. a) High-angle annular dark-field (HAADF) image of $GBVO_{0.02}$ particle, b) Bi, c) V, d) In, and e) Mo detectred by elemental mapping. f) HR-TEM image of $GBVO_{0.02}$ particle.

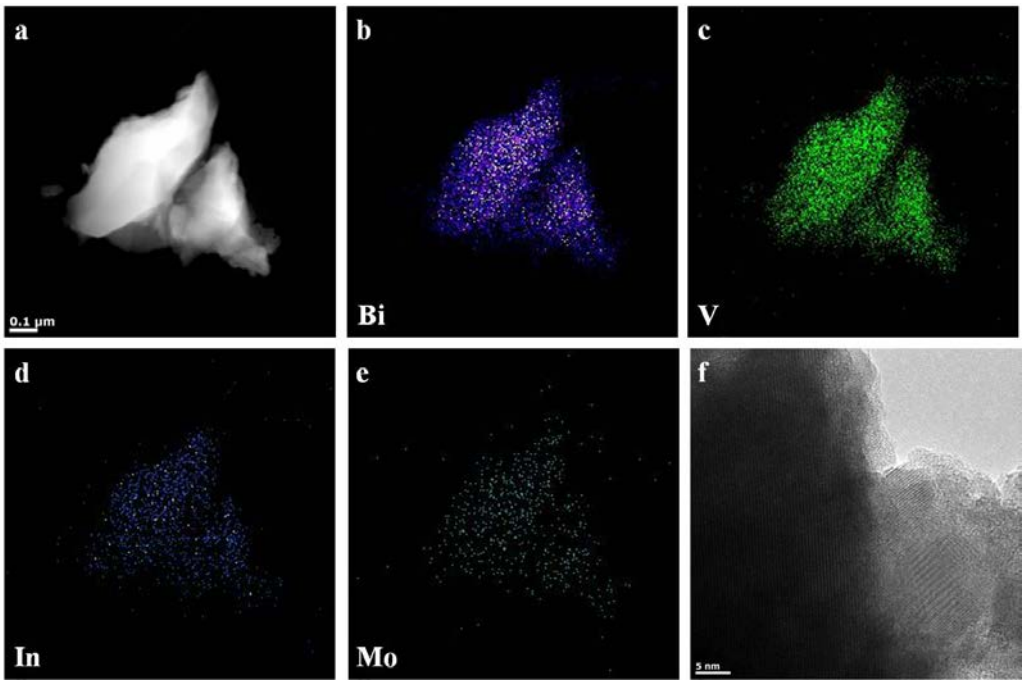

Figure S8. HR-TEM EDS analysis of $GBVO_{0.05}$. a) High-angle annular dark-field (HAADF) image of $GBVO_{0.05}$ particle. b) Bi, c) V, d) In, and e) Mo detectred by elemental mapping. f) HR-TEM image of $GBVO_{0.05}$ particle.

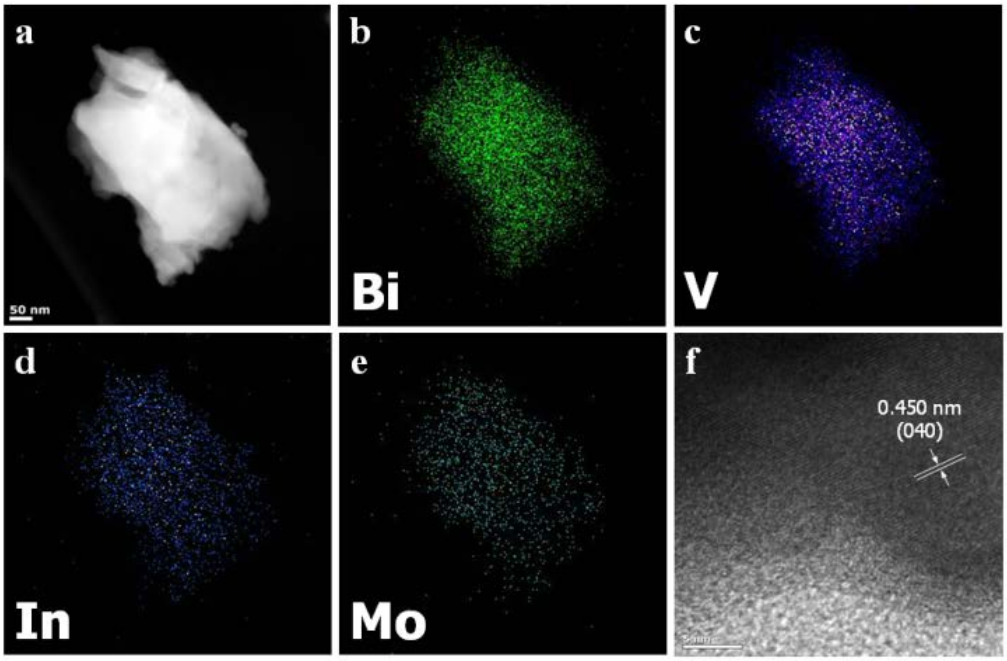

Figure S9. HR-TEM EDS analysis of $GBVO_{0.10}$. a) High-angle annular dark-field (HAADF) image of $GBVO_{0.10}$ particle. b) Bi, c) V, d) In, and e) Mo detected by elemental mapping. f) HR-TEM image of $GBVO_{0.10}$ particle.

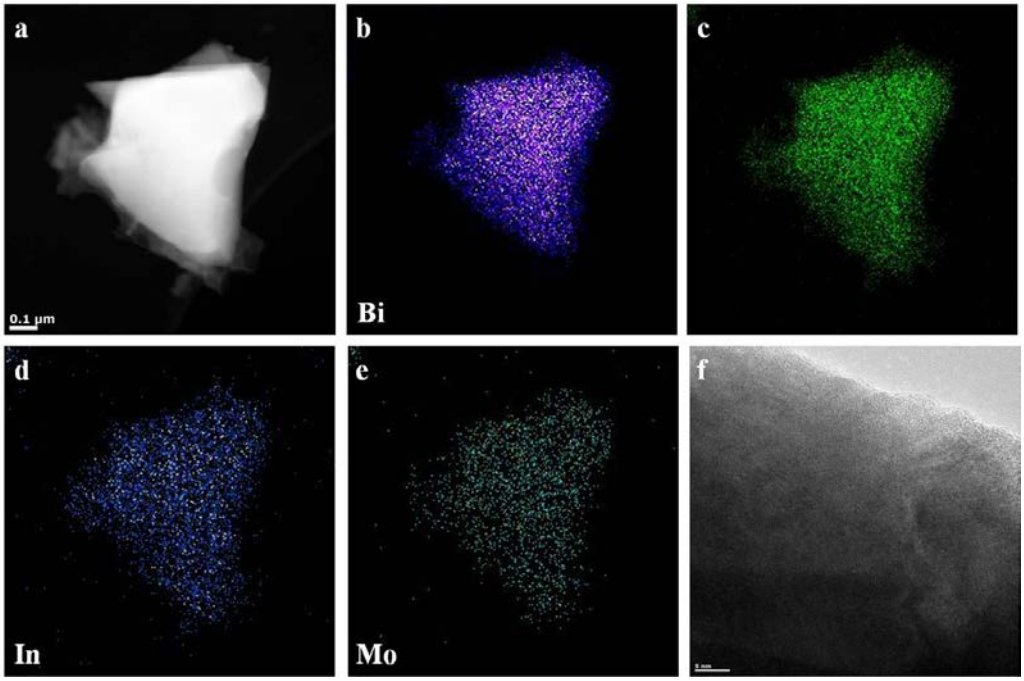

Figure S10. HR-TEM EDS analysis of $GBVO_{0.15}$. a) High-angle annular dark-field (HAADF) image of $GBVO_{0.15}$ particle. b) Bi, c) V, d) In, and e) Mo detectred by elemental mapping. f) HR-TEM image of $GBVO_{0.15}$ particle.

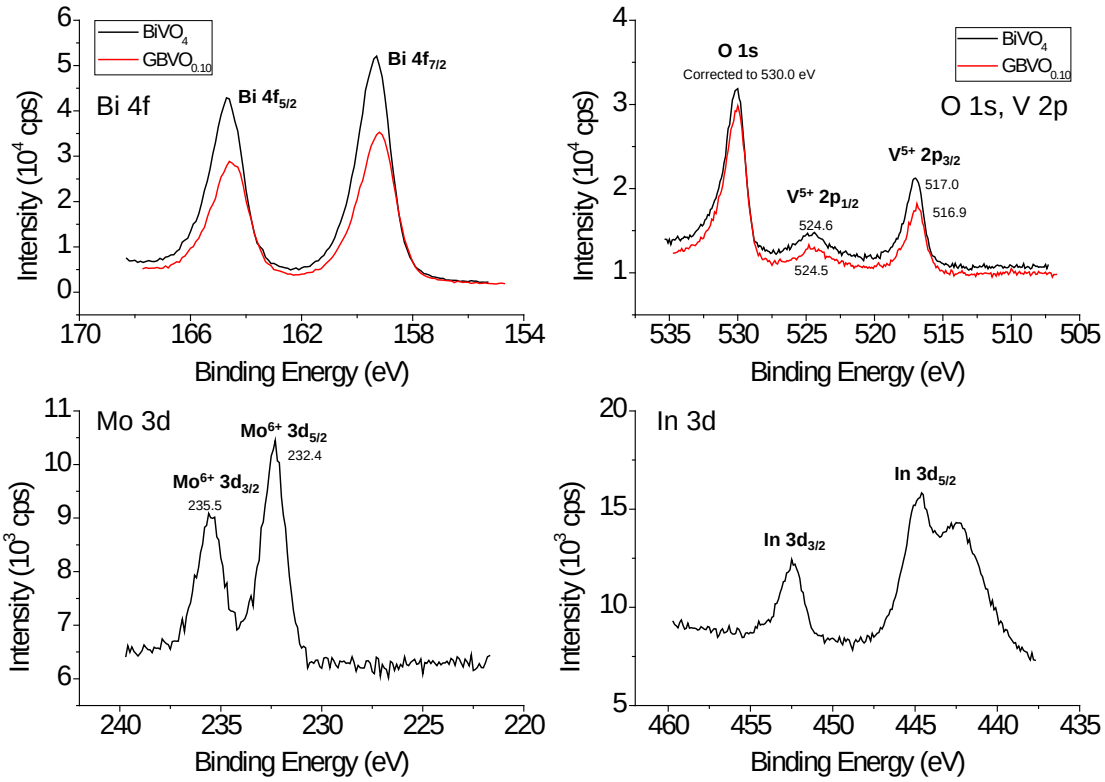

Figure S11. XPS of $GBVO_{0.10}$. The binding energies indicate that the involved elements are all in their stable oxidation states of Bi^{3+}, V^{5+}, Mo^{6+}, and In^{3+}.

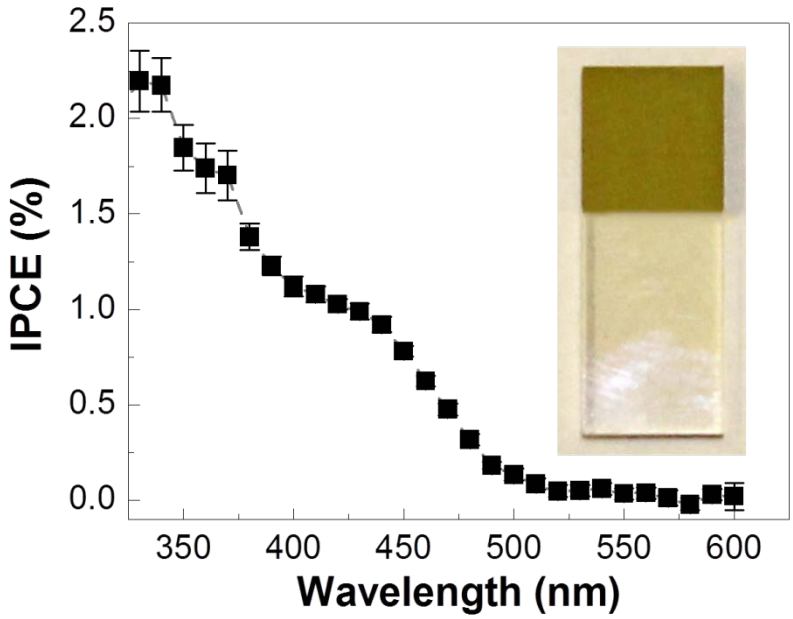

Figure S12. IPCE of $GBVO_{0.10}$ film. IPCE of $GBVO_{0.10}$ photoelectrode was measured at 0.7 V (vs. Ag/AgCl) in 0.5M Na_2SO_4 solution. The backside of $GBVO_{0.10}$ photoelectrode was illuminated with QEX7 (PV Measurements, Inc.) calibrated by a NIST-certified Si photodidode.

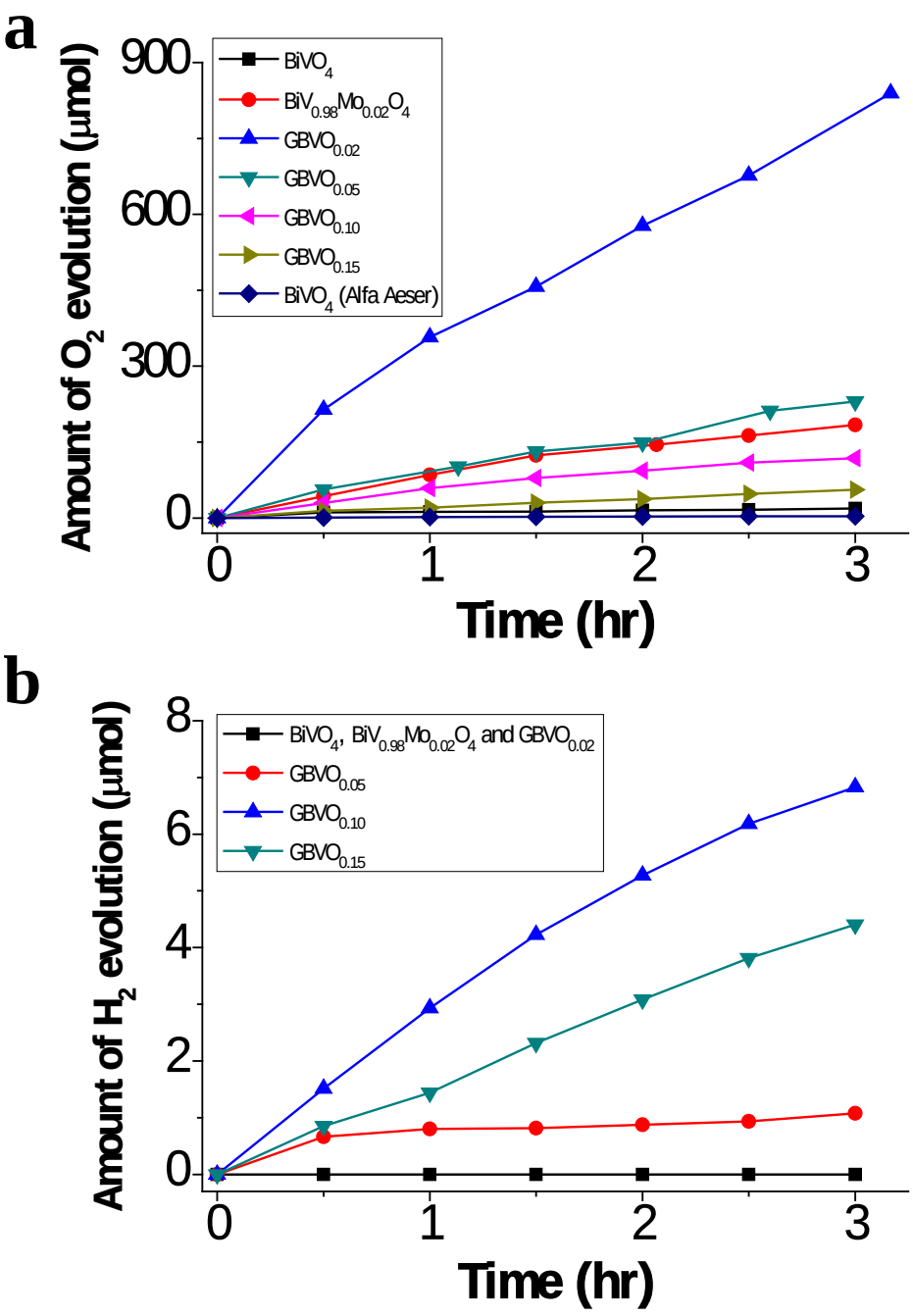

Figure S13. Photocatalytic activities of $GBVO_x$ with sacrificial reagents. a) Photocatalytic water oxidation by pristine $BiVO_4$, $BiV_{0.98}Mo_{0.02}O_4$ and all $GBVO_x$ samples under the visible-light ($\lambda \geq 420$ nm) irradiation. 0.1 g of photocatalyst powder was dispersed in 100 ml of aqueous $AgNO_3$ solution (50 mM) as an electron scavenger. b) Photocatalytic water reduction by pristine $BiVO_4$, $BiV_{0.98}Mo_{0.02}O_4$ and all $GBVO_x$ samples under the visible-light ($\lambda \geq 420$ nm) irradiation. 0.1 g of photocatalyst powder was dispersed in 80 ml of distilled water and 20 ml of CH_3OH as a hole scavenger.

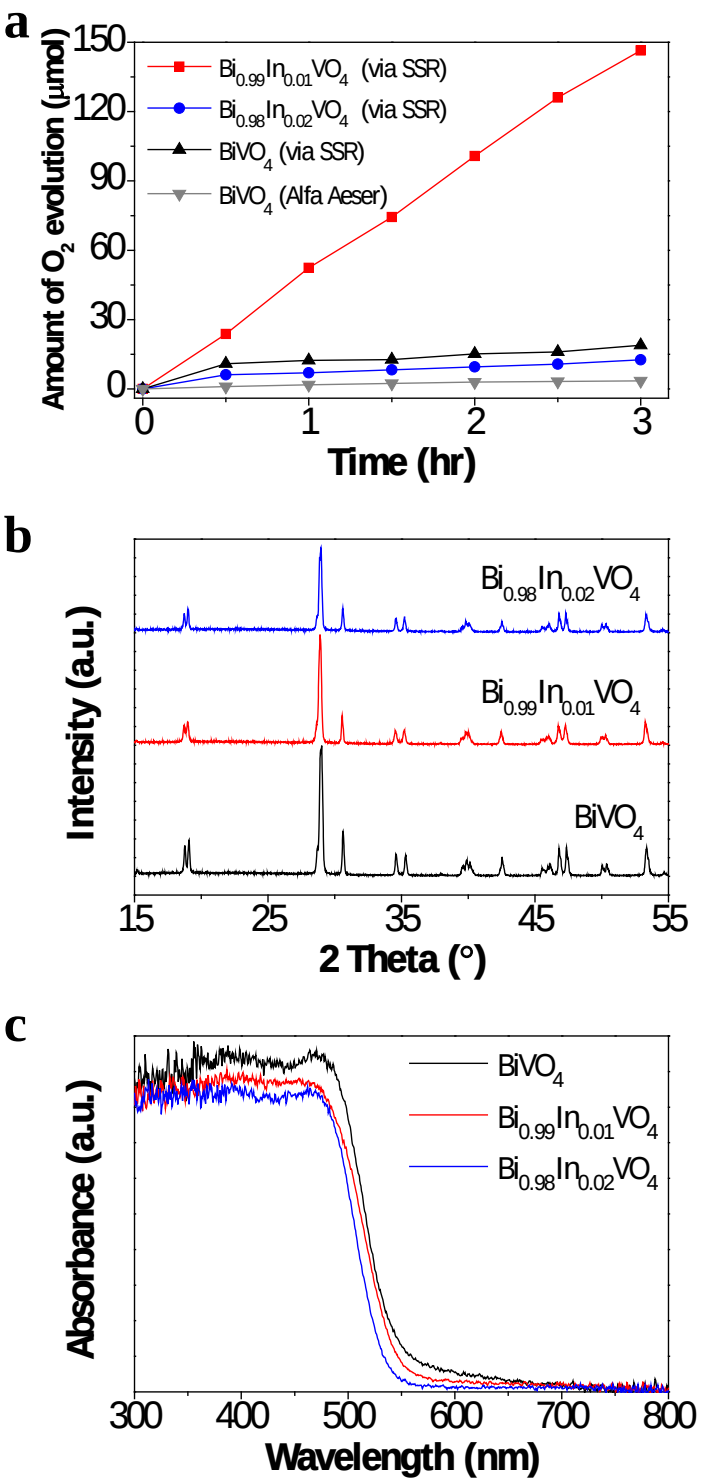

Figure S14. Single In-doped $BiVO_4$, $Bi_{1-x}In_xVO_4$. a) Photocatalytic water oxidation under the visible-light ($\lambda \geq$ 420 nm) irradiation. 0.1 g of photocatalyst powder was dispersed in 100 ml of aqueous $AgNO_3$ solution (50 mM) as an electron scavenger. b) XRD patterns, c) UV-Vis absorption spectra.

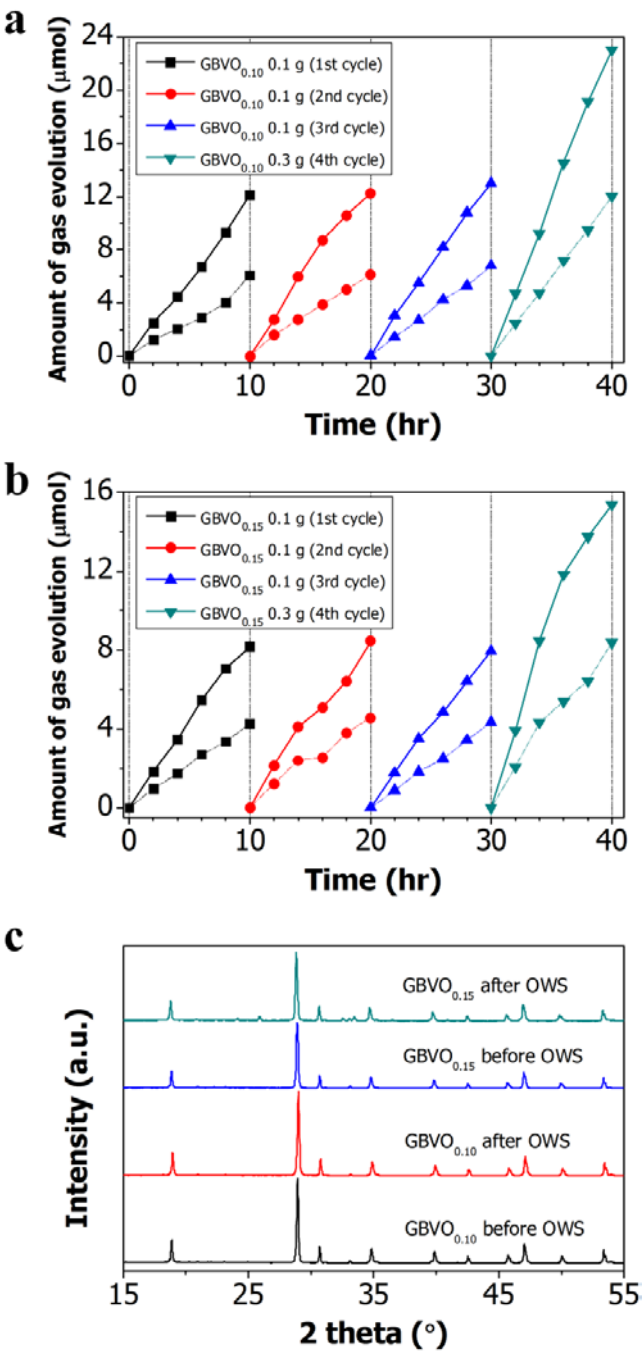

Figure S15. 40-hour overall water splitting by unmodified $GBVO_{0.10 \text{ and } 0.15}$ under the visible-light ($\lambda \geq 420$ nm) irradiation in order to test photochemical stability. a) Overall water splitting by unmodified $GBVO_{0.10}$, b) Overall water splitting by unmodified $GBVO_{0.15}$. Both overall water splitting reactions used N_2 purged suspension of 0.1 or 0.3 g photocatalyst powder in 100 ml distilled water. Solid and dashed lines indicate evolved H_2 and O_2, respectively. c) XRD patterns of $GBVO_{0.10 \text{ and } 0.15}$ before and after 40-hour overall water splitting reaction.

Supplementary Table

Table S1. ICP results of the four $GBVO_x$ samples.

Sample	Element	Wt %	Atomic %	Composition
2% In, Mo doped $BiVO_4$	In	0.82	0.024	**$Bi_{0.998}In_{0.024}V_{0.980}Mo_{0.020}O_4$**
	Mo	0.58	0.020	
5% In, Mo doped $BiVO_4$	In	1.84	0.055	**$Bi_{0.945}In_{0.055}V_{0.949}Mo_{0.051}O_4$**
	Mo	1.42	0.051	
10% In, Mo doped $BiVO_4$	In	3.63	0.114	**$Bi_{0.886}In_{0.114}V_{0.889}Mo_{0.111}O_4$**
	Mo	2.95	0.111	
15% In, Mo doped $BiVO_4$	In	5.52	0.181	**$Bi_{0.819}In_{0.181}V_{0.823}Mo_{0.177}O_4$**
	Mo	4.51	0.177	

Table S2. The estimated carrier density (N_D) of $BiVO_4$ and $GBVO_{0.05,\ 0.10\ and\ 0.15}$ electrodes.

The N_D values of BiVO4 and $GBVO_{0.05,\ 0.10\ and\ 0.15}$ electrodes are estimated by using previously reported method (7).

Electrode material	N_D /cm^3
$BiVO_4$	1.285E+21
$GBVO_{0.05}$	1.810E+20
$GBVO_{0.10}$	9.155E+19
$GBVO_{0.15}$	7.080E+19

References for Supporting Information

1. Kuhn HJ, Braslavsky SE, Schmidt R (2004) Chemical actinometry (IUPAC technical report). *Pure Appl Chem* 76(12): 2105-2146.
2. Montalti M, Credi A, Prodi L, Gandolfi MT (2006) Chemical Actinometry. *Handbook of Photochemistry* (Taylor & Francis Group LLC, Boca Raton, Florida), 3rd Ed, pp 601-616.
3. Sasaki Y, Iwase A, Kato H, Kudo A (2008) The effect of co-catalyst for Z-scheme photocatalysis systems with an Fe3+/Fe2+ electron mediator on overall water splitting under visible light irradiation. *J Catal* 259(1): 133-137.
4. Cullity BD (1978) Structure of Polycrystalline Aggregates. *Elements of X-ray diffraction* (Addison-Wesley, Reading, Massachusetts), 2nd Ed, pp 281-323.
5. Burton AW, Ong K, Rea T, Chan IY (2009) On the estimation of average crystallite size of zeolites from the Scherrer equation: A critical evaluation of its application to zeolites with one-dimensional pore systems. *Microporous Mesoporous Mater* 117(1-2): 75-90.
6. Williamson GK, Hall WH (1953) X-ray line broadening from filed aluminium and wolfram. *Acta Metallurgica* 1(1): 22-31.
7. Parmar KPS, et al. (2012) Photocatalytic and photoelectrochemical water oxidation over metal-doped monoclinic BiVO4 photoanode. *ChemSusChem* 5(10): 1926-1934.